

# Multilevel Boost Converter with Fractional Order PI-based MPPT Controller for Photovoltaic Applications

Anil Kumar Vemula<sup>1\*</sup>, Arounassalame Mouttou<sup>2</sup>

<sup>1,2</sup>Department of Electrical and Electronics Engineering, Pondicherry Engineering College, Pondicherry, India  
E-mail: vemula\_anil@yahoo.co.in

Received: February 15, 2020

Revised: March 27, 2020

Accepted: March 29, 2020

**Abstract** – A multilevel boost converter (MLBC) with fractional order- proportional integral (FO-PI)-based perturb and observe (P&O) maximum power point tracking (MPPT) controller is proposed to enhance the performance of photovoltaic (PV) systems. Two control schemes for the MLBC were investigated: i) MLBC with FO-PI-based P&O MPPT controller and ii) MLBC with only P&O MPPT controller. The simulation results, carried out using MATLAB/SIMULINK package, show that the performance of the MLBC with FO-PI-based P&O MPPT controller much over weights that of the MLBC with only P&O MPPT controller in terms of rise time, peak overshoot and settling time. These results indicate that the proposed system constitutes a good candidate for implementation in PV applications, in order to extract maximum electric power and to supply high output voltage to the load.

**Keywords** – Multilevel boost converter; Fractional order controller; Maximum power point tracking; Solar photovoltaic module; Small-signal model.

## 1. INTRODUCTION

As the world is facing environmental issues, climatic crises and depletion of fossil fuels, solar energy becomes very attractive option for electricity generation by means of photovoltaic (PV) systems. In recent years, these systems are getting progressively more importance because they are pollutant free and require less maintenance [1]. However, the output voltage of solar PV cells is significantly low and, hence, stepping it up is necessary to utilize the electric power efficiently [2, 3]. This can be achieved by utilizing a boost converter. But the voltage gain of ordinary boost converter is limited and it is not possible to obtain high voltage gain without stressing the switch. To overcome the drawbacks of conventional boost converters, a novel high step-up DC-DC multi-level boost converter (MLBC) is used [4]. Compared to conventional boost converter, MLBC has many advantages such as low switching frequency, low voltage stress, high voltage gain and efficiency [5, 6]. Since the electric power output from PV modules changes due to intermittent weather conditions like irradiance and temperature [7], various maximum power point tracking (MPPT) techniques are utilized to extract maximum power from PV modules. Among these MPPT techniques, perturb and observe (P&O) MPPT is the most popular due to its merits such as the good performance and the ease of implementation [8, 9].

Conventional proportional integral (PI) controllers were used traditionally to control power electronic converters under varying input/load conditions [10-12]. PI controllers are not robust and have less degree of freedom [13]. Fractional order (FO) controllers, on the other hand, are very efficient to achieve good transient and steady state response - compared to conventional controllers - because they have additional tuning parameter, which provides robustness under closed loop operation [14, 15].

\* Corresponding author

In this paper, a PV-fed MLBC with FO-PI-based P&O MPPT controller is proposed to enhance the performance of PV electric power generation system by reducing the output voltage ripples and accelerating transient and steady state responses and its performance is compared with that of a MLBC with only P&O MPPT.

The rest of the paper is organized as follows: section 2 presents a description of the solar PV scheme with high gain MLBC and FO-PI- based MPPT controller. Modeling of solar PV cells is presented in Section 3. P&O MPPT algorithm is explained in Section 4. The MLBC is presented in Section 5. A brief introduction about the FO controller is presented in Section 6. Simulation of MLBC with FO-PI-controlled MPPT is presented in Section 7. Conclusions are given in Section 8.

## 2. SYSTEM DESCRIPTION

Fig. 1 shows the block diagram of the proposed control and regulation scheme of the PV fed MLBC. The PV module contains PV cells which convert the solar energy into DC electric energy. To step up the low voltage obtained from the PV module, a MLBC is used. To extract maximum power and get better output performance from the system, FO-PI-based P&O MPPT controller is used. Here the reference voltage ( $V_{ref}$ ) is obtained from P&O MPPT and compared with the output voltage ( $V_o$ ), or fraction of  $V_o$ , of the converter. The difference/error value is sent to the FO-PI controller. The output of FO-PI controller is compared with the repeating sequence to generate the pulses.

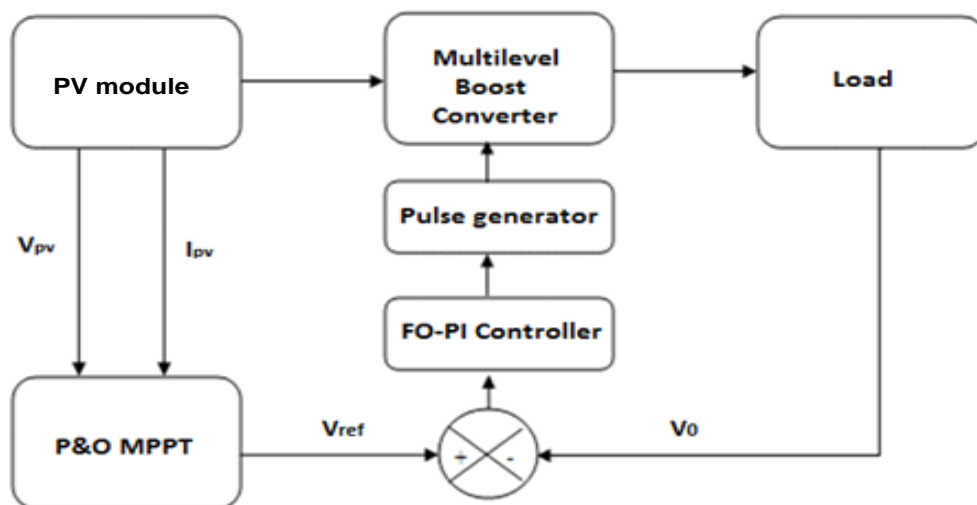


Fig. 1. Block diagram of the proposed scheme.

## 3. MODEL OF SOLAR PV CELL

A solar PV cell is used to convert the energy of sunlight into DC current by photovoltaic effect. In order to meet the energy requirements, a PV module is formed from solar PV cells, connected either in parallel or in series. Performance of the PV module is affected by many factors like temperature, irradiance, etc. The MATLAB/ Simulink model of a solar PV cell is shown in Fig. 2.

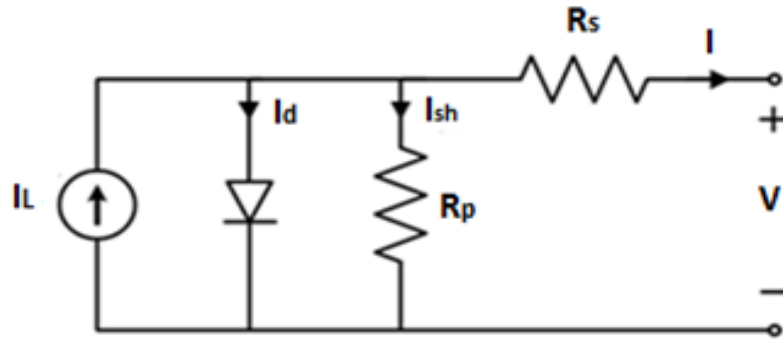


Fig. 2. Model of solar PV cell.

The mathematical equation which describes the current-voltage (I-V) characteristic of ideal solar PV cell is:

$$I = I_{pv,cell} - I_{0,cell} \left[ \exp\left(\frac{qV}{\alpha kT}\right) - 1 \right] \quad (1)$$

where  $k$  is Boltzmann constant,  $T$  is temperature of the p-n junction,  $I_{pv,cell}$  is the generated current by the incident light,  $\alpha$  is diode ideality constant,  $I_{0,cell}$  is reverse saturation current, and  $q$  is the electron charge.

A modified form of Eq. (1) that includes additional parameters is given by:

$$I = I_{pv,cell} - I_{0,cell} \left[ \exp\left(\frac{V + R_s I}{V_t \alpha} - 1\right) - \frac{V + R_s I}{R_p} \right] \quad (2)$$

where  $V_t = kT/q$  - is thermal voltage of the solar PV cell,  $R_p$  and  $R_s$  are the equivalent shunt and series resistances of the solar PV cell, respectively.

The saturation current of the solar PV cell is given by:

$$I_{0,cell} = \frac{I_{sc,n} + K_i \Delta T}{\exp\left(\frac{V_{oc,n} + K_v \Delta T}{\alpha V_t}\right)} \quad (3)$$

where  $I_{sc,n}$  is the nominal short-circuit current,  $V_{oc,n}$  is the nominal open-circuit voltage,  $K_v$  and  $K_i$  are the coefficients of voltage and current.

$$I_{pv} = (I_{pv,n} + K_i \Delta T) \frac{G}{G_n} \quad (4)$$

where  $I_{pv,n}$  is the generated nominal current  $\Delta T = T - T_n$ ,  $G_n$  and  $G$  are nominal and surface irradiation, respectively.

$$I_L = I_{pv} - I_d \quad (5)$$

#### 4. MPPT TECHNIQUE

Since the performance of PV modules is dependent on atmospheric conditions like temperature and irradiance, their characteristics are non-linear. Therefore, MPPT algorithms are used to track the maximum operating point on I-V characteristic to extract the maximum possible electric power from PV modules. Among different MPPT techniques, P&O MPPT is widely used due to its good performance and ease of its implementation. So in the proposed

- in this paper - system, P&O MPPT is designed and used to track the maximum power point on the I-V characteristic of the solar PV cell's model. Flow chart of the P&O algorithm is given in Fig. 3.

In this algorithm, the PV power changes due to slight perturbation. Perturbation continues in the same direction if the power increases, otherwise it would reverse. The algorithm gives reference voltage of the module according to peak voltage. This reference voltage is compared with the output voltage and difference/error voltage is generated. The FO-PI controller along with PWM generation scheme produces pulses with required duty cycle.

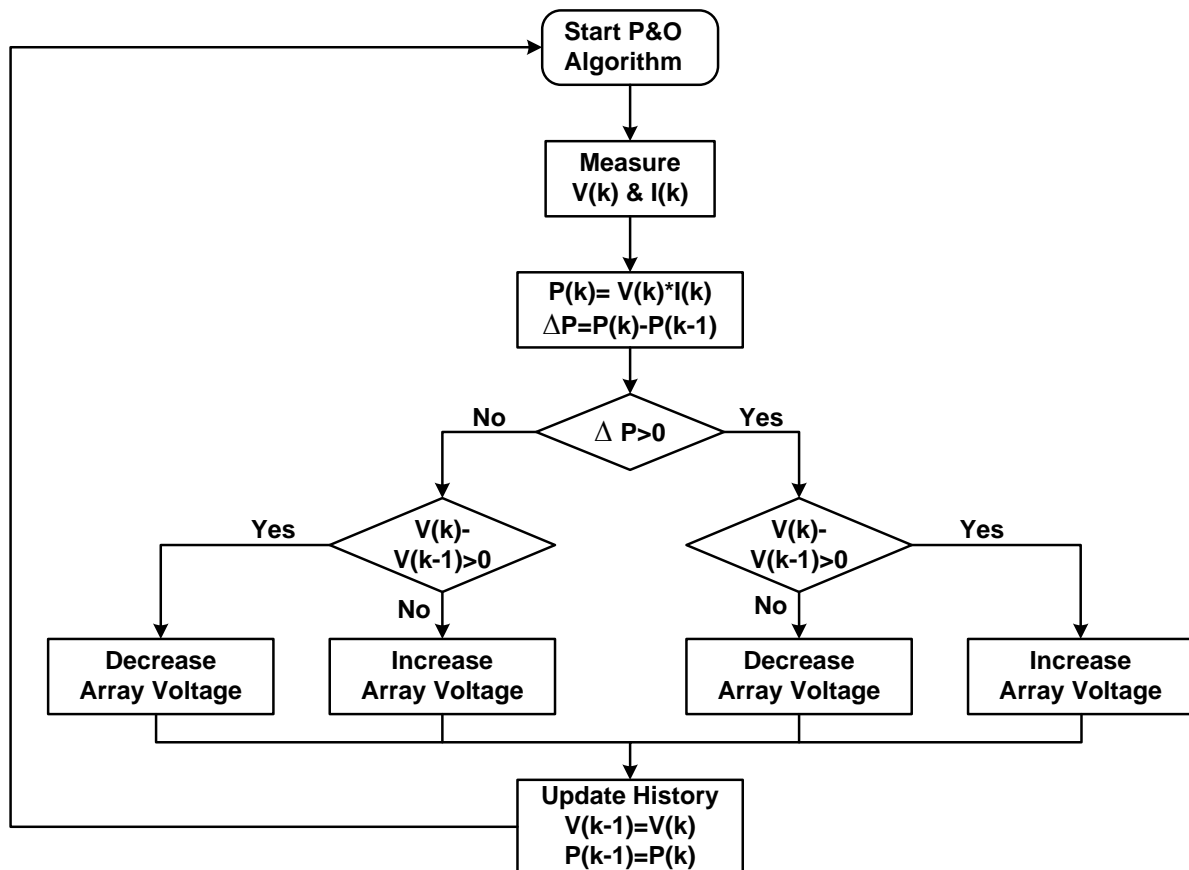


Fig. 3. Flow chart of P&O MPPT.

## 5. THE MULTILEVEL BOOST CONVERTER

DC-DC multilevel converters are very useful in high voltage applications and they are a key part of renewable energy systems. The merits of multi-level DC-DC converter over conventional ones are: 1) low voltage stress, 2) low switching frequency, 3) low electromagnetic interference noise, 4) less harmonic distortion, and 5) high efficiency [4]. MLBC is a combination of boost converter and switched capacitor circuit. For a MLBC to generate N levels in the yield voltage, it should have one switch,  $2N-1$  capacitors and  $2N-1$  diodes and one inductor [16]. A circuit of two-level boost converter with  $N=2$  is given in Fig. 4.

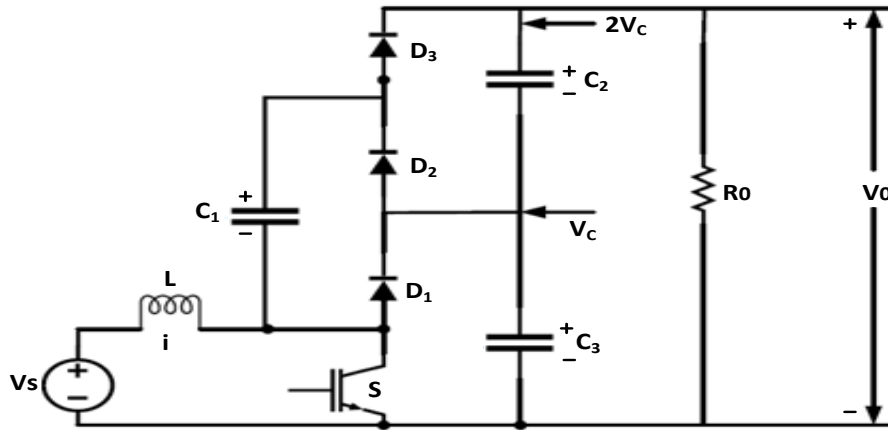


Fig. 4. Circuit of Multilevel boost converter.

The output DC voltage of N level MLBC with duty ratio  $d$  and input voltage  $V_s$  is:

$$V_0 = \frac{N \times V_s}{1-d} \quad (6)$$

The capacitor and inductor values to reduce ripples at the output of MLBC, is given by the following two equations:

$$C_1 = C_2 = C_3 = \frac{V_0}{\Delta V_s \times F_s \times R_0} \quad (7)$$

$$L_{\min} = \frac{5 \times (R_0(1-d)^2) d T_s}{N^2} \quad (8)$$

where  $R_0$  is load resistance,  $F_s$  is the switching frequency and  $T_s = 1/F_s$  is switching period.

The operation of the circuit is similar to the conventional boost converter with extra boosting of voltage by the multiplier circuit. During the ON state condition of the switch, the inductor is connected to the input source voltage. If the voltage across capacitor  $C_1$  is greater than the voltage across  $C_2$ , then  $C_2$  gets charged from  $C_1$  through  $D_2$  and switch  $S$ . During the OFF state condition of the switch, the inductor voltage adds up with the source voltage to charge the capacitor  $C_1$  through  $D_3$ . If the voltage across  $C_2$  is more than the voltage across capacitor  $C_3$ ,  $D_1$  conducts and the capacitors  $C_3$  and  $C_1$  are charged. The output voltage of two level boost converter is given by:

$$V_0 = \frac{2 \times V_s}{1-d} \quad (9)$$

### 5.1. Reduced Order Model of Two Level Boost Converter

It is very complex to determine the small-signal model for the two level boost converter as it has three capacitors and one inductor [17]. The number of states becomes four and the modeling of the original system results in a fourth order system. Instead of considering all the state variables for modeling, it is better to reduce the number of state variables under consideration by combining the values of capacitors based on the operation of the circuit during the ON and OFF conditions. So, the reduced order model is used for simplicity by considering the equivalent capacitances during the ON and OFF states of the switches. The equivalent circuit diagram of the reduced order models for the ON state of the switch is given

in Fig. 5. During the ON state of the switch the equivalent circuit has capacitors  $C_1$  and  $C_3$  in parallel and hence, they can be reduced into a single capacitance  $C_{1eq} = C_1 + C_3$ .

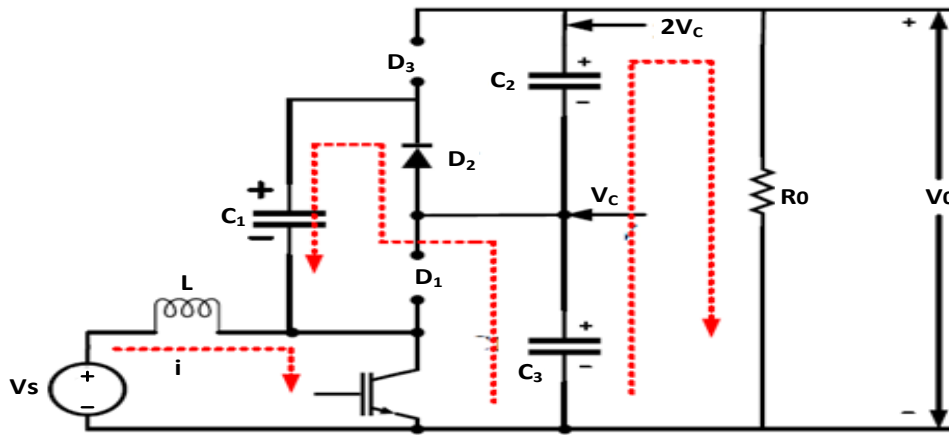


Fig. 5. Reduced order equivalent circuit of the two level converter (ON State).

The voltage across each capacitor at the output will be considered as the output voltage divided by the number of levels:

$$V_{C1} \cong V_{C2} \cong V_{C3} \cong \dots \cong V_{CN} \cong \frac{V_0}{N} \cong V_C \tag{10}$$

From the equivalent circuit of Fig. 5, the input and the output loops are completely separated. The KCL equations for these two loops are given in Eqs. (11) and (12).

$$L \frac{di}{dt} = V_s \tag{11}$$

$$C_{1eq} \frac{dV_c}{dt} = -\frac{N}{R_0} \times V_c \tag{12}$$

here N is the number of levels which is equal to 2.

During the OFF state of the switch, the equivalent circuit has the capacitors  $C_2$  and  $C_3$  in parallel, and hence they can be replaced by a single capacitance  $C_{2q} = C_1 + C_2$ . From the equivalent circuit of Fig. 6, it is obvious that the input and output loops are connected.

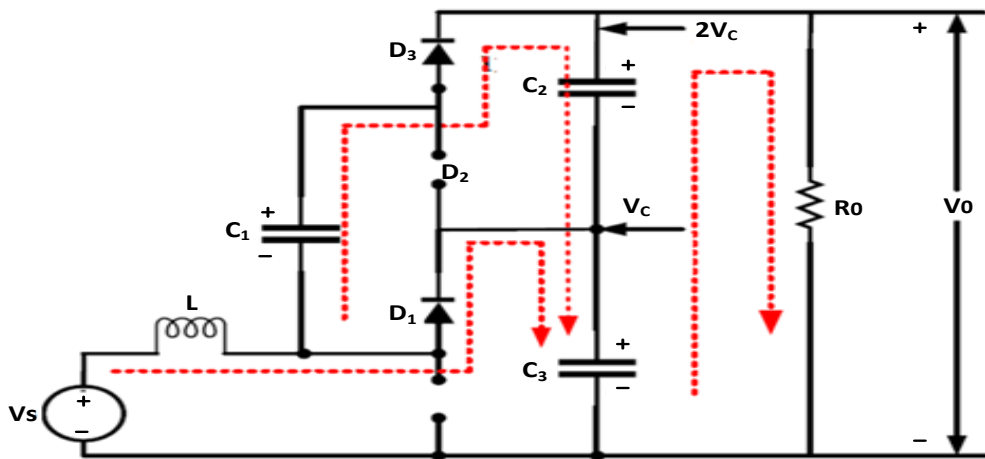


Fig. 6. Reduced order equivalent circuit of the two level converter (OFF state).

The KCL equations for these two loops are given in Eqs. (13) and (14).

$$L \frac{di}{dt} = -\frac{V_0}{N} + V_s \quad (13)$$

$$C_{2eq} \frac{dV_c}{dt} = i - \frac{N}{R_0} \times V_c \quad (14)$$

From Eqs. (11 - 14)

$$L \frac{di}{dt} = -(1-d) \frac{V_c}{N} + V_s \quad (15)$$

$$C_{eq} \frac{dV_c}{dt} = (1-d)i - \frac{N}{R_0} \times V_c \quad (16)$$

here  $C_{eq} = C_{1eq} + C_{2eq}$

From Eqs. (15) and (16), the state space matrix is formulated and is given as:

$$\begin{bmatrix} \frac{di}{dt} \\ \frac{dV_c}{dt} \end{bmatrix} = \begin{bmatrix} 0 & -\frac{(1-d)}{N \times L} \\ \frac{(1-d)}{C_{eq}} & -\frac{N}{R_0 C_{eq}} \end{bmatrix} \begin{bmatrix} i \\ V_c \end{bmatrix} + \begin{bmatrix} \frac{1}{L} \\ 0 \end{bmatrix} V_s \quad (17)$$

The output equations are given in Eqs. (18-20) as:

$$V_0 = V_c \quad (18)$$

$$I_g = i \quad (19)$$

$$\begin{bmatrix} V_0 \\ I_g \end{bmatrix} = \begin{bmatrix} 0 & 1 \\ 1 & 0 \end{bmatrix} \begin{bmatrix} i \\ V_c \end{bmatrix} \quad (20)$$

## 5.2. Small-Signal Modeling of The Two Level Boost Converter

To derive the small-signal model of the two level boost converter, the following small-signal components are added:  $d = d + \hat{d}$ ,  $V_0 = V_0 + \hat{v}_0$ ,  $i = I + \hat{i}$ ,  $V_c = V_c + \hat{v}_c$ ,  $V_s = v_s + \hat{v}_s$  and  $i_g = I_g + \hat{i}_g$ . Substituting these components in Eqs. (17) and (20) and separating the steady state, the small-signal quantities are derived and given in the following two equations:

$$\begin{bmatrix} \frac{\hat{d}i}{dt} \\ \frac{\hat{d}v_c}{dt} \end{bmatrix} = \begin{bmatrix} 0 & -\frac{(1-d)}{N \times L} \\ \frac{(1-d)}{C_{eq}} & -\frac{N}{R_0 C_{eq}} \end{bmatrix} \begin{bmatrix} \hat{i} \\ \hat{v}_c \end{bmatrix} + \begin{bmatrix} 0 & \frac{\hat{d}}{N \times L} \\ -\frac{\hat{d}}{C_{eq}} & 0 \end{bmatrix} \begin{bmatrix} i \\ V_c \end{bmatrix} + \begin{bmatrix} \frac{1}{L} \\ 0 \end{bmatrix} \hat{v}_s + \begin{bmatrix} 0 \\ -\frac{1}{C_{eq}} \end{bmatrix} \hat{i}_g \quad (21)$$

$$\begin{bmatrix} \hat{v}_0 \\ \hat{i}_g \end{bmatrix} = \begin{bmatrix} 0 & 1 \\ 1 & 0 \end{bmatrix} \begin{bmatrix} \hat{i} \\ \hat{v}_c \end{bmatrix} \quad (22)$$

Combining the above matrices yields:

$$\begin{bmatrix} \frac{d\hat{i}}{dt} \\ \frac{d\hat{v}_c}{dt} \end{bmatrix} = \begin{bmatrix} 0 & -\frac{(1-d)}{N \times L} \\ \frac{(1-d)}{C_{eq}} & -\frac{N}{RC_{eq}} \end{bmatrix} \begin{bmatrix} \hat{i} \\ \hat{v}_c \end{bmatrix} + \begin{bmatrix} \frac{1}{L} & 0 & \frac{V_c}{N \times L} \\ 0 & -\frac{1}{C_{eq}} & \frac{i_L}{C_{eq}} \end{bmatrix} \begin{bmatrix} \hat{v}_s \\ \hat{i}_g \\ \hat{d} \end{bmatrix} \quad (23)$$

$$\begin{bmatrix} \hat{v}_0 \\ \hat{i}_g \end{bmatrix} = \begin{bmatrix} 0 & 1 \\ 1 & 0 \end{bmatrix} \begin{bmatrix} \hat{i} \\ \hat{v}_c \end{bmatrix} \quad (24)$$

The transfer function between the output voltage and duty ratio can be determined by:

$$\frac{\hat{v}_0}{\hat{d}} = C(sI - A)^{-1} B_3 \quad (25)$$

$$\text{where } C = [0 \ 1], \quad A = \begin{bmatrix} 0 & -\frac{(1-D)}{N \times L} \\ \frac{(1-D)}{C_{eq}} & -\frac{N}{R_0 C_{eq}} \end{bmatrix}, \quad B_3 = \begin{bmatrix} \frac{V_c}{N \times L} \\ i \\ C_{eq} \end{bmatrix}$$

After substituting the matrix values of A, B<sub>3</sub> (third column in Eq. (23) and C in Eq. (25), we get the small-signal transfer function model of the high gain boost converter that is given in the following equation:

$$\frac{\hat{v}_0}{\hat{d}} = \frac{\frac{(1-d)V_0}{N \times L} - \frac{s \times i}{C_{eq}}}{s^2 + \frac{s \times N}{RC_{eq}} + \frac{(1-d)^2}{N \times L \times C_{eq}}} \quad (26)$$

## 6. FRACTIONAL PI CONTROLLER

In process control applications, proportional-integral-derivative (PID) controllers are extensively used because of their low percentage of overshoot, design simplicity and low settling time. PID controllers can be enhanced by using suitable settings for the fractional-I and fractional-D actions. A PID controller, comprised of an integrator of order  $\lambda$  and a

differentiator of order  $\mu$ , is known as fractional order PID (FO-PID) controller ( $P I^\lambda D^\mu$ ). The block diagram of FO-PID controller is shown in Fig. 7.

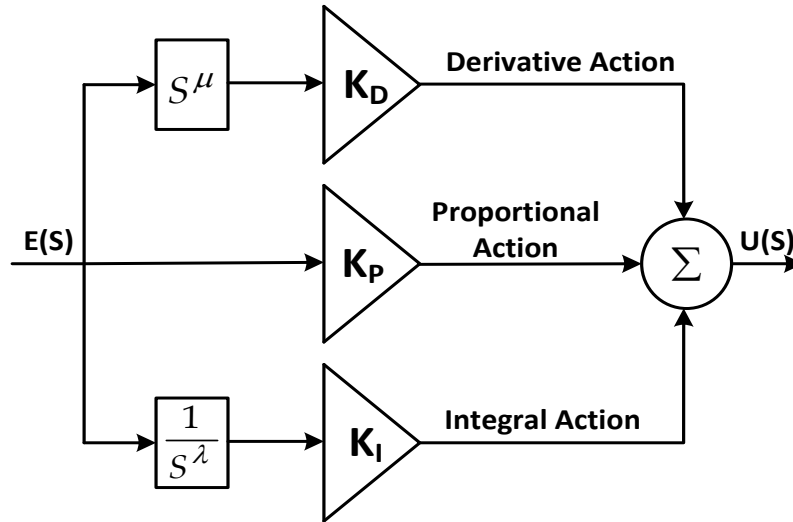


Fig. 7. FO-PID controller.

The transfer function of the FO-PID controller can be written as follows:

$$G_C(s) = K_P + \frac{K_I}{s^\lambda} + K_D s^\mu \quad (27)$$

where  $\lambda$  and  $\mu > 0$ .

FO-PID controllers have additional tuning parameters like  $\lambda$  and  $\mu$ . This provides robustness under closed loop operation. To obtain a FO-PI controller from the FO-PID,  $K_d$  and  $\mu$  are considered to be zero [18].

The transfer function of the FO-PI controller ( $PI^\lambda$ ) is:

$$G_C(s) = K_P + K_I/s^\lambda \quad (28)$$

Parameters of the high gain MLBC are given in Table 1. The transfer function of two level boost converter after substituting the parameters of the system, presented by Eq. (26) is expressed as:

$$\frac{V_0}{d} = \frac{480 - 466 \cdot 67s}{s^2 + 4.44s + 1111 \cdot 11} \quad (29)$$

The FO-PI controller can be designed for the above transfer function using FOMCON toolbox of MATLAB. The tuning parameters of FO-PI controller obtained by the FOMCON toolbox are  $K_p=0.8$ ,  $K_i=8$ ,  $\lambda=0.6$ . FOMCON toolbox is used to calculate and optimize the parameters of the FO-PID controller. The target here is to minimize the performance metric, i.e. integral of square error (ISE). The minimization of ISE will result in reduced rise time and decrease in settling time. The transfer function of the FO-PI controller which is going to be used for the control of the two level boost converter is given in Eq. (30):

$$TF(FO - PI) = 0.8 + \frac{8}{s^{0.6}} \quad (30)$$

The simulation is carried out using MATLAB/SIMULINK and the performance of the two level converter is analyzed with the designed fractional order controller.

## 7. SIMULATION RESULTS

Parameters of the MLBC (N=2) and the PV module used in the present investigation are given in Tables 1 and 2, respectively. Simulation of the circuit with the controller is carried out in MATLAB/SIMULINK.

Table 1. MLBC (N=2) specifications.

Parameter	Value
Switching frequency	25 KHz
Inductor	25 mH
Capacitors	1500 $\mu$ F
Load resistance	100 $\Omega$

Table 2. PV module parameters.

Parameter	Value
Open-circuit voltage	24 V
Short-circuit current	3.87 A
Temperature	298 K
Solar irradiance	1000 W/m <sup>2</sup>

Performance (in terms of output voltage, current and power) of MLBC with FO-PI-based P&O MPPT controller is compared to that of MLBC with only P&O MPPT controller. The results, depicted in Figs. 8-10, prove that the response of the MLBC with P&O MPPT controller has less overshoot but still takes more time to reach steady state value. But the time response of MLBC with FO-PI-based P&O MPPT controller is much better, i.e., the overshoot is lower and the response settles much faster.

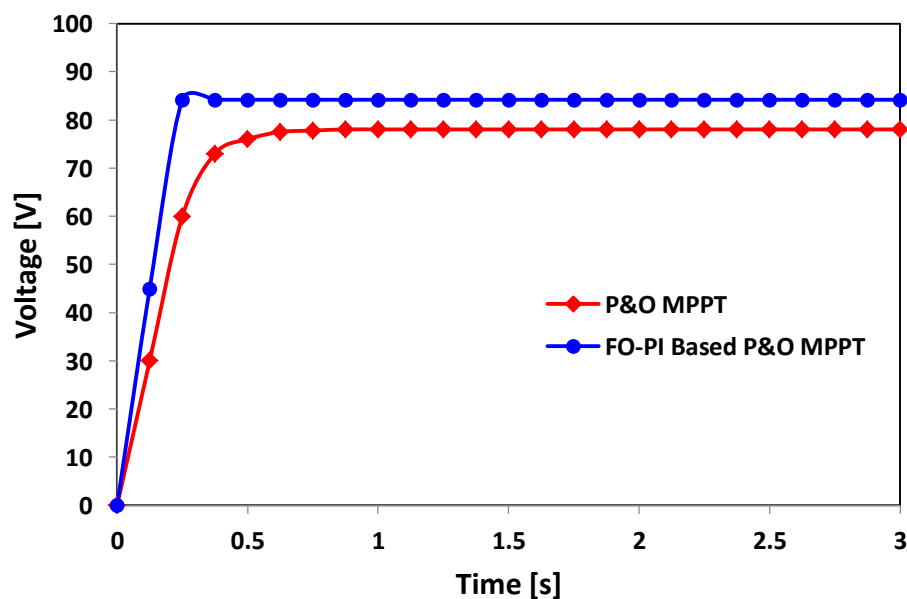


Fig .8. Output voltage of the MLBC with the two investigated control schemes.

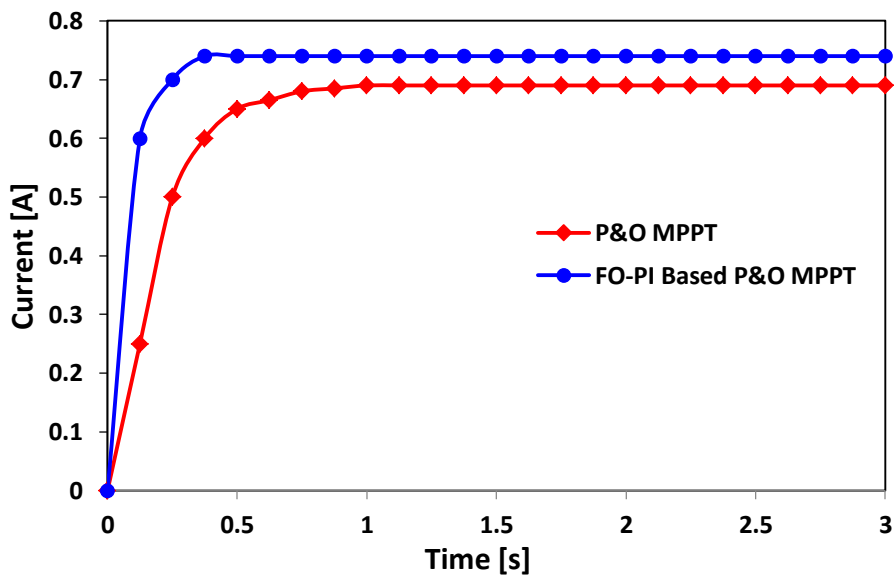


Fig .9. Output current of the MLBC with the two investigated control schemes.

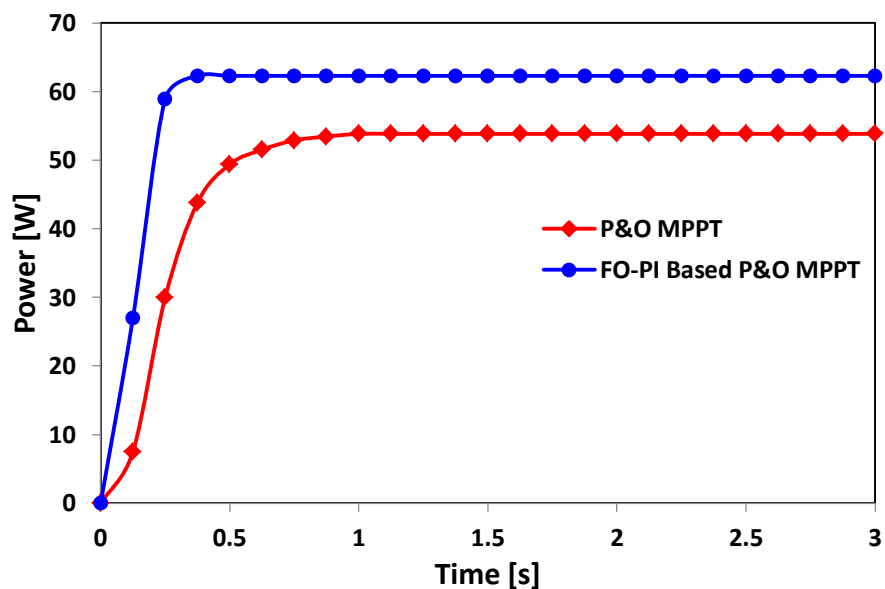


Fig .10. The output power of the MLBC with the two investigated control schemes.

Table 3 gives the output values of the MLBC with P&O MPPT and with FO-PI-based P&O MPPT techniques. It shows that the MLBC with FO-PI-based MPPT controller gives higher output voltage and power. Table 4 gives the results of time domain specifications of the outputs of MLBC with P&O MPPT technique and with FO-PI-based P&O MPPT technique. It reveals that the output response of the MLBC with FO-PI-based P&O MPPT technique has faster rise and settling times. Ripple factor for the P&O MPPT technique is 0.096% and for the proposed FO-PI-based P&O MPPT is 0.387%, meaning that the output waveform of the proposed system has more ripples. Hence, the proposed system derives more output power from the PV modules. The response of the system is very fast and steady state is achieved in less time. But the ripples in the output are more in the present case.

Table 3. Output of MLBC with different techniques.

Technique	Input voltage	Output voltage	Output current	Output power
	V	V	V	W
P&O MPPT	24	78.04	0.69	53.94
FO-PI-controlled P&O MPPT	24	84.2	0.74	62.22

Table 4. Performance parameters for output voltage with different techniques.

Parameter	P&O MPPT	FO-PI-controlled MPPT
Maximum overshoot	0	0
Settling time [s]	0.85	0.25
Rise time [s]	0.35	0.2
Ripple factor [%]	0.096	0.387

## 8. CONCLUSIONS

In this paper, a MLBC with FO-PI-based P&O MPPT controller is proposed for PV applications. The performance of the proposed system is compared with that of MLBC with only P&O MPPT controller. The MLBC with FO-PI-based MPPT controller gives desired output voltage and power with reduced distortions. The power output from the proposed MLBC with the FO-PI-based P&O MPPT controller is much better than that obtained from the MLBC with only P&O MPPT controller. The output response of the proposed system is much faster (i.e settling time is 0.25 sec) than that of the MLBC with only P&O MPPT controller (i.e. settling time is 0.85 sec). Hence, the proposed FO-PI-based P&O MPPT controller is much better than the conventional P&O MPPT controller for MLBC circuit. The proposed system will be very useful for implementation in PV applications in order to extract maximum power and to supply constant high output voltage to the load. However, ripple factor for the converter with only P&O MPPT technique is 0.096% and for the proposed converter with FO-PI-based P&O MPPT is 0.387%. Indicating that the proposed system has more ripples in the output waveform. This is a drawback that will be further investigated in future research works.

## REFERENCES

- [1] M. Villalva, J. Gazoli, E. Filho, "Modeling and circuit-based simulation of photovoltaic arrays," *Proceedings of 2009 Brazilian Power Electronics Conference*, Bonito-Mato Grosso do Sul, pp. 1244-1254, 2009.
- [2] M. Kasper, D. Bortis, J. Kolar, "Classification and comparative evaluation of PV panel-integrated DC-DC converter concepts," *IEEE Transactions on Power Electronics*, vol. 29, no. 5, pp. 2511-2526, 2013.
- [3] Singh, S. N, "Selection of non-isolated DC-DC converters for solar photovoltaic system," *Renewable and Sustainable Energy Reviews*, vol. 76, pp. 1230-1247, 2017.
- [4] J. Rosas-Caro, J. Ramírez, P. García-Vite, "Novel DC-DC multilevel boost converter," *Proceedings of 2008 IEEE Power Electronics Specialists Conference*, Rhodes, pp. 2146-2151, 2008.
- [5] A. Ghosh, S. Saran, "High gain DC-DC step-up converter with multilevel output voltage," *Proceedings of 2018 International Symposium on Devices, Circuits and Systems*, Howrah, pp. 1-6, 2018.

- [6] A. Musale, B. Deshmukh, "Three level DC-DC boost converter for high conversion ratio," *Proceedings of 2016 International Conference on Electrical, Electronics, and Optimization Techniques*, Chennai, pp. 643-647, 2016.
- [7] A. Ali, M. Saied, M. Mostafa, T. Abdel-Moneim, "A survey of maximum PPT techniques of PV systems," *Proceedings of 2012 IEEE Energytech*, Cleveland, OH, pp. 1-17, 2012.
- [8] D. Sera, L. Mathe, T. Kerekes, S. Spataru, R. Teodorescu, "On the perturb-and-observe and incremental conductance MPPT methods for PV systems," *IEEE Journal of Photovoltaics*, vol. 3, no. 3, pp. 1070-1078, 2013.
- [9] B. Alajmi, K. Ahmed, S. Finney, B. Williams, "A maximum power point tracking technique for partially shaded photovoltaic systems in micro grids," *IEEE Transactions on Industrial Electronics*, vol. 60, no. 4, pp. 1596-1606, 2013.
- [10] J. Reddy, S. Sonar, "Closed loop control of multi level DC-DC boost converter," *International Journal of Engineering and Advanced Technology*, vol. 9, no. 2, pp. 4512-4518, 2019.
- [11] L. Bulla, V. Nattarasu, "Comparison of different control techniques for three level DC-DC boost converter," *International Research Journal of Engineering and Technology*, vol. 3, no. 7, pp. 1-4, 2016.
- [12] P. Sharma, P. Kumar, H. Sharma, N. Pal, "Closed loop controlled boost converter using a PID controller for solar wind power system installation," *International Journal of Engineering and Technology*, vol. 7, no. 2.8, pp.255-260, 2018.
- [13] K. Alam, A. Hoque, "Design and analysis of closed loop interleaved boost converter with arduino based soft PI controller for photovoltaic application," *Proceedings of 2019 IEEE International Conference on Electrical, Computer and Communication Technologies*, Coimbatore, India, pp. 1-5, 2019.
- [14] I. Birs, C. Muresan, I. Nascu, C. Ionescu, "A Survey of recent advances in fractional order control for time delay systems," *IEEE Access*, vol. 7, pp. 30951-30965, 2019.
- [15] H. Ren, J. Fan, O. Kaynak, "Optimal design of a fractional-order proportional-integer-differential controller for a pneumatic position servo system," *IEEE Transactions on Industrial Electronics*, vol. 66, no. 8, pp. 6220-6229, 2019.
- [16] J. Mayo-Maldonado, R. Salas-Cabrera, J. Rosas-Caro, J. Deleon-Morales, E. Salas-Cabrera, "Modelling and control of DC-DC multilevel boost converter," *IET Power Electronics*, vol. 4, no. 6, pp. 693-700, 2011.
- [17] J. Mayo-Maldonado, J. Rosas-Caro, R. Salas-Cabrera, A. González-Rodríguez, O. Ruíz-Martínez, R. Castillo-Gutiérrez, J. Castillo-Ibarra, H. Cisneros-Villegas, "State space modeling and control of the dc-dc multilevel boost converter," *Proceedings of 2010 20th International Conference on Electronics Communications and Computers*, Cholula, pp. 232-236, 2010.
- [18] Y. Chen, I. Petras, D. Xue, "Fractional order control- a tutorial," *Proceedings of 2009 IEEE American Control Conference*, St. Louis, MO, pp. 1397-1411, 2009.